An Analytical Model of Electron Mobility for Strained-Si Channel nMOSFETs*

Li Xiaojian†, Tan Yaohua, and Tian Lilin

(*Tsinghua National Laboratory for Information Science and Technology, Institute of Microelectronics, Tsinghua University, Beijing* 100084, *China*)

Abstract: An analytical model of electron mobility for strained-silicon channel nMOSFETs is proposed in this paper. The model deals directly with the strain tensor, and thus is independent of the manufacturing process. It is suitable for 〈100〉/〈110〉 channel nMOSFETs under biaxial or 〈100〉/〈110〉 uniaxial stress and can be implemented in conventional device simulation tools.

Key words: Strained-Si; electron mobility; analytical model; nMOSFET; uniaxial stress/strain
PACC: 7220F; 7340Q **EEACC**: 2530F; 2560B
CLC number: TN301.1 **Document code**: A **Article ID**: 0253-4177(2008)05-0863-06

1 Introduction

Having crossed the 65nm node, technology to induce strain into a channel has become a necessary to enhance the electron mobility in a channel, which falls quickly as the critical size decreases.

The modeling of electron mobility in a strained channel nMOSFET has been studied for a long time[1~3], but most models are based on specific technologies like SiGe substrate[4~6]. Since the method to induce strain is still studied and continuously improved, we need a process-independent model to meet these situations.

Dhar and Enzo[7] have developed a mobility model that deals directly with strain tensor and thus, is independent of the manufacturing process and can be applied to 〈100〉 bulk Si materials. They give an improved model that is also suitable for 〈110〉 bulk Si materials[8]. Two points of their model should be noted. First, the model can only be used to calculate the bulk Si mobility. Second, the treatment of the 〈110〉 direction is somewhat simple. In this paper, we suggest a new electron mobility model, based on the model of Dhar and Enzo[7], for a strained Si channel nMOSFET. In this model, we can calculate not only the mobility of bulk Si, but also that of the strained channel, and we improve the treatment of the 〈110〉 direction over[8].

2 Modeling

2.1 Model structure

In this model, the total mobility can be obtained by taking the weighted average of mobility tensors of each valley, expressed as

$$\hat{\mu} = \sum_{i=1}^{3} p^{(i)} \cdot \hat{\mu}_{\mathrm{n}}^{(i)} \tag{1}$$

Here $\hat{\mu}$ is the mobility tensor, $p^{(i)}$ is the population of the ith valley (considering the symmetry of Si conduction band, the six conduction band valley can be treated as three equivalent classes sorted by axis, and i is the class index), and $\hat{\mu}^{(i)}$ is the mobility tensor of the ith valley.

The mobility tensor of a single valley can be expressed as a product of scalar mobility and scaled inverse effective mass tensor[7]

$$\hat{\mu}^{(i)} = \mu \hat{m}_{(i)}^{-1}, \quad i = x, y, z \tag{2}$$

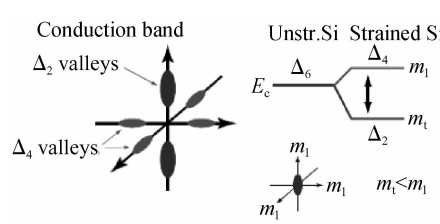

Fig. 1 Demonstration of the effects of stress on energy band[10]

* Project supported by the Special Funds for Major State Basic Research Projects (No. 2006CB302705)
† Corresponding author. Email: lixj03@mails.tsinghua.edu.cn
Received 26 November 2007, revised manuscript received 9 January 2008

in which μ is the scalar mobility obtained by average effective mass and $\hat{m}_{(i)}^{-1}$, which will be discussed in section 2.3, is the effective mass correction tensor that represents the difference of effective mass for different directions.

The scalar mobility is

$$\frac{1}{\mu} = \frac{1}{\mu_{\text{equiv}}} + \frac{1}{\mu_{\text{nequiv}}} + \frac{1}{\mu_{\text{ni}}} + \frac{D}{\mu_{\text{ac}}} + \frac{D}{\mu_{\text{sr}}} + \frac{D}{\mu_{\text{cit}}} \quad (3)$$

Here μ_{equiv}, μ_{nequiv}, μ_{ni}, μ_{ac}, μ_{sr} and μ_{cit} denote intravalley scattering and intervalley scattering between the equivalent valley, intervalley scattering between the nonequivalent valley, impurity scattering, additional surface phonon scattering, surface roughness scattering, and interface coulomb scattering, respectively. These scattering terms are summed according to Mathiessen's rule, and D denotes the vanishing term as the channel depth from the Si-SiO_2 interface increases.

2.2 Model details

(1) Phonon Scattering: The contribution of the phonon is evaluated by μ_{equiv} and μ_{nequiv} [7]. According to Ref. [7], μ_{equiv} can be expressed as a constant. μ_{nequiv} is a function of stress,

$$\mu_{\text{nequiv}}^{(i)} = \mu_{\text{nequiv}}^{0} / h^{(i)} \quad (4)$$

Here μ_{nequiv}^{0} evaluates the effect of intervalley phonon scattering between a nonequivalent valley where no stress exists, and $h^{(i)}$ is the dimension factor of the ith valley under strain

$$h^{(i)} = \frac{g\left(\frac{\Delta_{ij}^{\text{emi}}}{k_{\text{B}}T}\right) + g\left(\frac{\Delta_{il}^{\text{emi}}}{k_{\text{B}}T}\right) + \exp\left(\frac{\hbar\omega_{\text{opt}}}{k_{\text{B}}T}\right)\left[g\left(\frac{\Delta_{ij}^{\text{abs}}}{k_{\text{B}}T}\right) + g\left(\frac{\Delta_{il}^{\text{abs}}}{k_{\text{B}}T}\right)\right]}{2\left[g\left(\frac{-\hbar\omega_{\text{opt}}}{k_{\text{B}}T}\right) + \Gamma\left(\frac{3}{2}\right)\right]} \quad (5)$$

in which g has the form

$$g(z) = \begin{cases} \exp(-z)\cdot\Gamma(3/2) & \forall z > 0 \\ \exp(-z)\cdot\Gamma(3/2) & \forall z < 0 \end{cases} \quad (6)$$

Here Δ_{ij}^{emi} (Δ_{ij}^{abs}) is the phonon energy needed when an phonon is emitted (absorbed) from the $j(i)$th to $i(j)$th valley.

The effects of strain on μ_{nequiv} result from the strain induced valley splitting that change the energy needed for a phonon to be emitted or absorbed between nonequivalent valleys. Δ_{ij}^{emi} and Δ_{ij}^{abs} under strain can be expressed as

$$\begin{aligned} \Delta_{ij}^{\text{emi}} &= \Delta E_{\text{C}}^{(j)} - \Delta E_{\text{C}}^{(i)} - \hbar\omega_{\text{opt}} \\ \Delta_{ij}^{\text{abs}} &= \Delta E_{\text{C}}^{(j)} - \Delta E_{\text{C}}^{(i)} + \hbar\omega_{\text{opt}} \end{aligned} \quad (7)$$

where $\hbar\omega_{\text{opt}}$ is the phonon energy, and $\Delta E_{\text{C}}^{(i)}$ ($\Delta E_{\text{C}}^{(j)}$) denotes the strain induced splitting of the $i(j)$ th valley

$$\Delta E_{\text{c}}^{(i)} = \Xi_{\text{d}}(\varepsilon_{xx} + \varepsilon_{yy} + \varepsilon_{zz}) + \Xi_{\text{u}}\varepsilon_{ii} \quad (8)$$

Here, Ξ_{d}, Ξ_{u} are the dilatation and shear deformation potential, and ε_{ii} is the ith diagnose component in the strain tensor.

(2) Impurity Scattering: We assume that the impurity scattering is independent of stress. Thus, the μ_{ni} in the unstrained mobility model is appropriate for our strained Si mobility model.

In this model, we employ the Masetti model[11] to evaluate the effect of impurity, which is the default mobility model to deal with impurity in Sentaurus ①

$$\mu_{\text{ni}} = \mu_{\text{min1}}\exp\left(-\frac{P_{\text{c}}}{N_{\text{i}}}\right) + \frac{\mu_{\text{const}} - \mu_{\text{min2}}}{1 + \left(\frac{N_{\text{i}}}{C_{\text{r}}}\right)^{\alpha}} + \frac{\mu_1}{1 + \left(\frac{C_{\text{s}}}{N_{\text{i}}}\right)^{\beta}} \quad (9)$$

Here, $N_{\text{i}} = N_{\text{A}} + N_{\text{D}}$ denotes the total concentration of ionized impurities. μ_{const} is the intrinsic mobilities. μ_{min1}, μ_{min2} and μ_1 are reference mobilities. P_{c}, C_{r}, and C_{s} are reference doping concentrations. The remaining variables are fitting parameters whose values can be found in Ref. [11].

Next, we use Dhar's method[7] to rewrite the expression,

$$\begin{aligned} \mu_{\text{b}}^{(i)} &= \frac{1}{\mu_{\text{equiv}}} + \frac{1}{\mu_{\text{nequiv}}} + \frac{1}{\mu_{\text{ni}}} \\ &= \frac{\beta\mu^{L}}{1 + (\beta - 1)h^{(i)} + \beta\left(\frac{\mu^{L}}{\mu_{\text{ni}}} - 1\right)} \end{aligned} \quad (10)$$

where $h^{(i)}$ is the dimension factor for stress in Eq. (4), μ^{L} is the low field mobility in Si, and β can be evaluated as

$$\beta = f \times \frac{m_{\text{t}}}{m_{\text{c}}} \quad (11)$$

in which f is the ratio between the mobility of the high stressed channel and the low field mobility. f is not a constant and is decided by the environment, which will be discussed in section 2.4. m_{t} and m_{c} denote the transverse normalized effective mass and average normalized effective mass, respectively. All normalized effective mass present in this paper are normalized to m_0.

(3) Surface Scattering: The effects of surface mainly result from the roughness of surface, surface charges, and other factors related to the environment. In this model, three types of surface effects are considered. They are additional surface phonon scattering (μ_{ac}), surface roughness scattering (μ_{sr}), and surface coulomb scattering (μ_{cit}). We employ the Lombardi model[11] (the Lombardi model is the default model to deal with interface degradation of mobility in Sentaurus) for the former two types of scattering,

$$\mu_{\text{ac}} = \frac{B}{F_{\perp}} + \frac{C(N_{\text{i}}/N_0)^{\lambda}}{F_{\perp}^{1/3}(T/T_0)^{k}} \quad (12)$$

① Sentaurus is the TCAD simulation platform from Synopsys .

$$\mu_{\rm sr} = \left(\frac{F_\perp^3}{\eta} + \frac{(F_\perp / F_{\rm ref})^{A^*}}{\delta}\right)^{-1} \tag{13}$$

where $F_\perp$ is the effective vertical electric field in units of V/cm, T is the temperature in units of K, $N_{\rm i}$ is the impurity density in units of $\rm cm^{-3}$, and $T_0 = 300\rm K$, $N_0 = 1\ \rm cm^{-3}$, $F_{\rm ref} = 1\rm V/cm$. The remaining parameters are fitted with the values found in Ref. [11].

Surface coulomb scattering is caused by the trap charges and the mobile/fixed charges, which are mostly positive near the gate-channel interface. As the effective vertical electric field increases, the channel electrons increase, screen the surface charge, and finally weaken the effect of surface coulomb scattering. According to Ref. [12], surface coulomb scattering induced mobility $\mu_{\rm cit} \propto \sqrt{N_{\rm inv}}/N_{\rm it}$, where $N_{\rm it}$ is the surface charge density and $N_{\rm inv}$ is the charge density in the inversion layer. The effective vertical field and charge density in the inversion layer are related by[13]

$$F_\perp = \frac{Q_{\rm dep} + \eta Q_{\rm inv}}{\varepsilon_{\rm Si}} \tag{14}$$

Here, $Q_{\rm dep}$ and $Q_{\rm inv}$ are the sheet charge density of the depletion layer and the inversion layer, respectively, $\varepsilon_{\rm Si}$ is the electric permittivity of Si, and η depends on the manufacturing process, usually 1/2 for electrons and 1/3 for holes.

Using these two relations, the surface coulomb scattering can be evaluated. However, the model obtained from the relationships above does not accord with the experimental results, and this disagreement can not be solved by simply adjusting parameters. Thus, to meet experimental results, we improve the relationship mathematically to

$$\mu_{\rm cit} = \mu_0 \left(\frac{1}{\ln(N_{\rm i}/N_0)} \times \frac{F_\perp}{N_{\rm it}}\right)^\alpha \left(\frac{T}{T_0}\right)^\beta \tag{15}$$

where μ_0 is the empirical mobility, and α, β, N_0, T_0 are parameters extracted from available experimental data.

Generally, surface effects are strongly related to position (mainly the distance to the Si-SiO_2 interface). As the distance increases, the surface effect is weakened. Thus, a diminishing factor is necessary. We employ expression[11]

$$D = \exp(-x/l_{\rm crit}) \tag{16}$$

for the modification. Here x is the distance to the Si-SiO_2 interface in units of nm, $l_{\rm crit}$ is the average diminishing distance whose values can be found in Ref. [11]. This diminishing factor acts directly on the term of surface scattering by multiplication

$$\frac{1}{\mu_{\rm surface}} = \frac{D}{\mu_{\rm ac}} + \frac{D}{\mu_{\rm sr}} + \frac{D}{\mu_{\rm cit}} \tag{17}$$

With the increase of distance, $\mu_{\rm surface}$ will be enhanced swiftly and its contribution to the total mobility will decline quickly.

(4) Relative Population: The relative population of the ith valley $p^{(i)}$ in Eq. (2) is approximated by

$$p^{(i)} \approx n_{\rm str}^{(i)} / \sum_{i=1}^{3} n_{\rm str}^{(i)} \tag{18}$$

where $n_{\rm str}^{(i)}$ is the electron density of the ith valley and $\sum_{i=1}^{3} n_{\rm str}^{(i)}$ is the total electron density.

The valley splitting induced by strain causes divergence in the electron density of each valley. We have

$$n_{\rm str}^{(i)} = N_{\rm c}^{(i)} \exp[-(E_{\rm C} - E_{\rm F})/k_{\rm B}T] \exp[-\Delta E_{\rm c}^{(i)}/k_{\rm B}T] \tag{19}$$

where $N_{\rm c}^{(i)}$ is the effective density of states for electrons in the ith valley, $E_{\rm c}$ is the conduction band edge of unstrained Si, $E_{\rm F}$ is the Fermi level, and $\Delta E_{\rm c}^{(i)}$ is the splitting of the valley with the same form as Eq. (8).

For a ⟨110⟩ stress, the effective density of states $N_{\rm c}^{(i)}$ will depend on strain, which will be discussed in the following section.

2.3 Channel direction

In this model, the default reference axis is parallel to ⟨100⟩, ⟨010⟩, and ⟨001⟩, and the default channel direction is ⟨100⟩. To calculate the mobility of other channel directions, like ⟨110⟩, going directly through the coordinate transformation of the results of the ⟨100⟩ channel will lead to a wrong answer. According to Ref. [9], electrons will have a higher mobility under ⟨110⟩ stress. The reason for this phenomenon is unclear, but there is a view that the influence of strain on effective mass of electron is anisotropic. The effective mass of the ⟨100⟩ direction of Δ_2 valleys is not sensitive to the strain, while that of the ⟨110⟩ direction is. With tensile strain, the effective mass of the ⟨110⟩ direction of Δ_2 valleys will decrease and the mobility will then rise.

The view above does have theoretical support. Energy band calculation has pointed out that under ⟨110⟩ stress, the shape of energy band in the ⟨110⟩ direction has a notable change that cannot be neglected[13,14]. Using nonlocal EPM, we calculated the modification of the z-valley effective mass correction tensor $\hat{m}_z^{-1}$ as

$$\hat{m}_z^{-1} = m_{\rm c} \begin{pmatrix} m_{\rm t}^{-1} & \Delta_{\varepsilon_{xy}}/2 & 0 \\ \Delta_{\varepsilon_{xy}}/2 & m_{\rm t}^{-1} & 0 \\ 0 & 0 & m_{\rm l}^{-1} \end{pmatrix} \tag{20}$$

Here $m_{\rm t}$ and $m_{\rm c}$ are the transverse normalized effective mass and average normalized effective mass in Eq. (11), $m_{\rm l}$ is the longitudinal normalized effective mass, and $\Delta_{\varepsilon_{xy}}/2$ gives the effective mass correction under stress as

$$\Delta_{\varepsilon_{xy}} = \frac{(\alpha + \beta\varepsilon_{xy}^2)\varepsilon_{xy}}{(\hbar^2 k_\varepsilon^2/2m_0)} \tag{21}$$

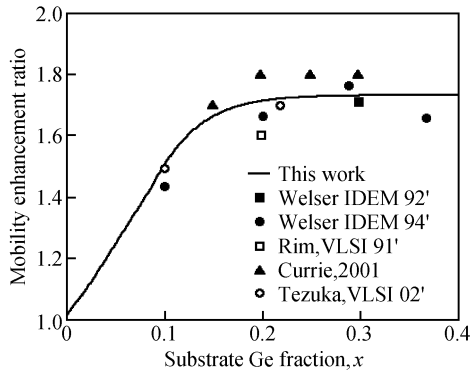

Fig. 2 Dependence of electron low field mobility on biaxial stress (T = 300K, $N_A = 10^{15}\,cm^{-3}$, $E_\perp$ = 0MV/cm, Ge fraction = 0～40%)

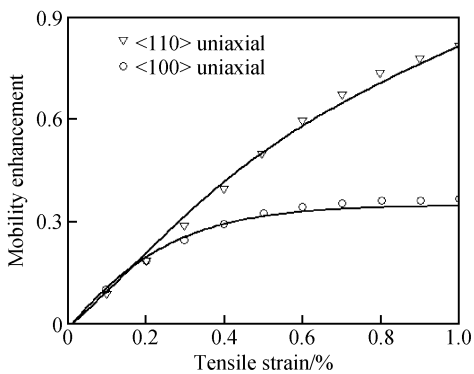

Fig. 3 Dependence of electron low field mobility on uniaxial stress (T = 300K, $N_A = 1.5\times10^{10}\,cm^{-3}$, $E_\perp$ = 0MV/cm, Tensile strain = 0～1%)

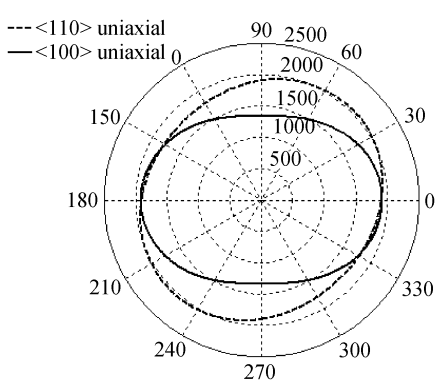

Fig. 4 Dependence of electron low field mobility (in $cm^2/(V\cdot s)$) on channel direction (T = 300K, $N_A = 1.5\times10^{10}\,cm^{-3}$, $E_\perp$ = 0MV/cm, Tensile strain = 0.4%)

where m_0 is the static mass of electron in units of kg, ε_{xy} is the component of strain tensor of no units and α, β, k_ε are fitting parameters with values in Table 1. a_0 in Table 1 is the lattice constant.

Table 1 Parameters for mass modification under stress

Parameter	Unit	Value
α	eV	20
β	eV	−3691.1
k_ε	$2\pi/a_0$	0.076

Using Eq. (20), we can write the normalized effective mass in the $\langle 110\rangle/\langle 1\bar{1}0\rangle$ direction

$$m_{110} = \frac{2m_t}{2+\Delta_{\varepsilon_{xy}}m_t}$$
$$m_{1\bar{1}0} = \frac{2m_t}{2-\Delta_{\varepsilon_{xy}}m_t} \quad (22)$$

Three points should be noted in our calculation. First, the results show changes of $\hat{m}_x^{-1}$ and $\hat{m}_y^{-1}$ are not significant and can be neglected. Second, changes of longitudinal effective mass m_l^{-1} in $\hat{m}_z^{-1}$ are also small enough to be neglected. Third, the modification of effective mass in z-valleys is only related to ε_{xy}.

The change of transverse effective mass not only influences the mass correction tensor $\hat{m}_i^{-1}$ in Eq. (2), but also alters the effective density of states N_c in Eq. (19) since $N_c \propto m_{dn}^{3/2}$. The effective mass of density of states m_{dn} is

$$m_{dn} = (S^2 m_l m_t^2)^{1/3} \quad (23)$$

According to these relations, a corrected term to express the change of N_c is

$$N'_c = N_c\left(\frac{m'_{dn}}{m_{dn}}\right)^{3/2} \quad (24)$$

where $m'_{dn} = (S^2 m_l m_t^{\parallel} m_t^{\perp})^{1/3}$.

2.4 Enhancement factor

The mobility enhancement factor f in Eq. (11) is an important parameter in this model. It is the ratio between the mobility of the high stressed channel and the low field mobility. According to Eq. [15], this factor is not constant but depends on the effective vertical electric field and the layer thickness of strained-silicon. Based on the data from Ref. [15], we modify f to

$$f = f(F_\perp, T_{Si}) = p_1(F_\perp)T_{Si}^2 + p_2(F_\perp)T_{Si} + p_3(F_\perp) \quad (25)$$

in which T_{Si} is the thickness of the strained-silicon layer in units of nm, $F_\perp$ is the effective vertical electric field intensity in units of V/cm, and p_1, p_2 and p_3 are parameters related to $F_\perp$.

3 Results and discussion

Figures 2～4 shows the influence of strain on low field mobility. Figure 2 represents the dependence of electron low field mobility on biaxial stress. Several results[16] have been compared, and the trend of this model accords well with these data. Figure 3 gives the dependence of electron low field mobility on uniaxial stress and the data from Uchida's work[9]. When the strain increases to about 0.4%, the mobility of the $\langle 100\rangle$ channel stops increasing, but that of $\langle 110\rangle$ channel continues to increase, although the rate of increase declines. Figure 4 shows the dependence of low

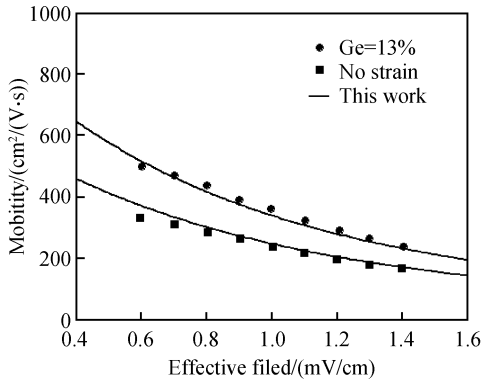

Fig. 5　Dependence of electron channel mobility on biaxial stress and effective electrical field (T = 300K, $N_A = 1.8 \times 10^{16}$ cm^{-3}, $E_\perp = 0.4 \sim 1.7$MV/cm, Ge fraction = 13%)

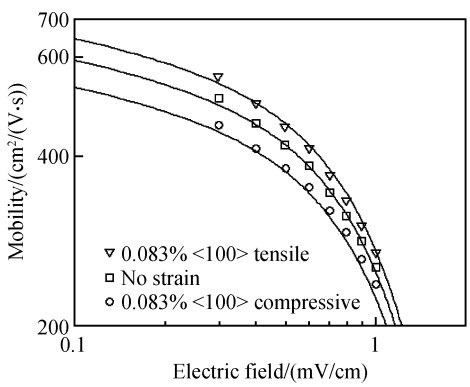

Fig. 6　Dependence of electron channel mobility on 〈100〉 uniaxial stress and effective electrical field (T = 300K, $N_A = 1.8 \times 10^{17}$ cm^{-3}, $E_\perp = 0 \sim 2$MV/cm, Tensile strain = -0.083%, 0, 0.083%)

field mobility on channel direction under stress of different directions.

Figures 5～7 show the channel electron mobility under the influence of both stress and vertical electric field. The comparison data comes from the work of Rim[17] and Uchida[18], respectively.

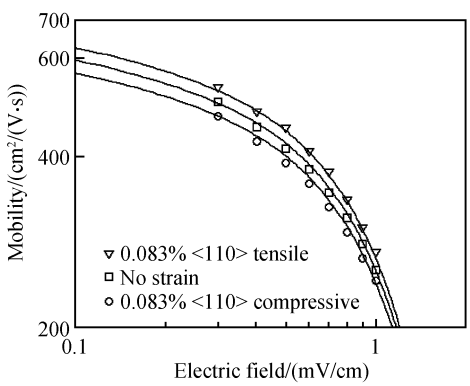

Fig. 7　Dependence of electron channel mobility on 〈110〉 uniaxial stress and effective electrical field (T = 300K, $N_A = 1.8 \times 10^{17}$ cm^{-3}, $E_\perp = 0 \sim 2$MV/cm, Tensile strain = -0.083%, 0, 0.083%)

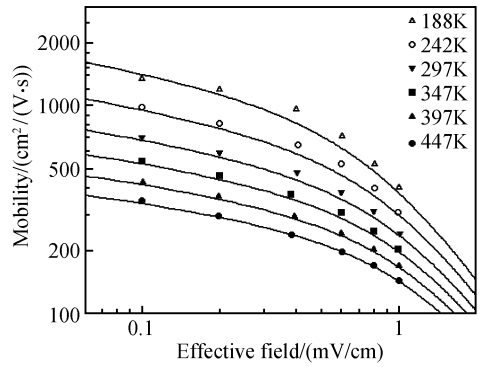

Fig. 8　Dependence of electron channel mobility on temperature and effective vertical electric field (T = 188, 242, 297, 347, 397, 447K, $N_A = 3.9 \times 10^{15}$ cm^{-3}, $E_\perp = 0 \sim 2$MV/cm)

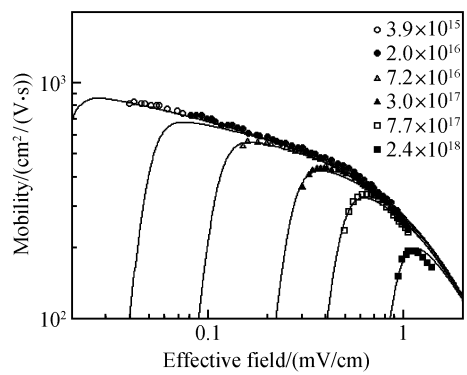

Fig. 9　Dependence of electron channel mobility on doping concentration and effective electric field (T = 300K, $N_A = 3.9 \times 10^{15}$, 2.0×10^{16}, 7.2×10^{16}, 3.0×10^{17}, 7.7×10^{17}, 2.4×10^{18} cm^{-3}, $E_\perp = 0 \sim 2$MV/cm)

Figures 8 and 9 show the dependence of channel electron mobility on temperature and doping concentration, respectively. The comparison data comes from the work of Takagi[19].

Figure 10 gives the dependence of the f factor on layer thickness of strain-silicon and effective vertical electric field. The comparison data comes from the work of Mizuno[15].

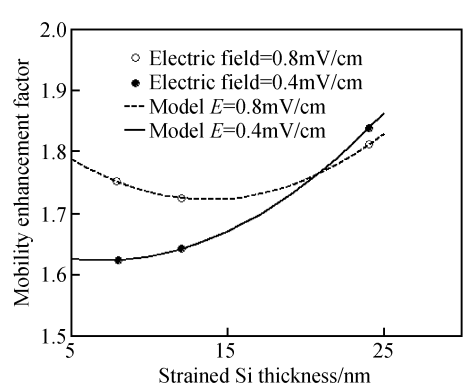

Fig. 10　Dependence of f factor on thickness of strain-Si layer and effective vertical electric field (T = 300K, $N_A = 1.5 \times 10^{10}$ cm^{-3}, $E_\perp = 0.4$, 0.8MV/cm)

4 Conclusion

An analytical model of electron mobility for strained-silicon channel nMOSFETs is proposed in this paper. The model is independent of the manufacturing process because it deals directly with the strain tensor. It can be applied to both 〈100〉 and 〈110〉 channel nMOSFETs. The model accords well with experimental results.

References

[1] People R, Bean J C, Lang D V, et al. Modulation doping in Ge_xSi_{1-x}/Si strained layer heterojunction. Appl Phys Lett, 1984, 45: 1231

[2] Jorke H, Herzog H J. Mobility enhancement in modulation-doped Si-$Si_{1-x}Ge_x$ superlattice grown by molecular beam epitaxy. The Electrochemical Society, 1985, 85: 352

[3] Bean J C. Strained-layer epitaxy of Ge_xSi_{1-x}/(Si, Ge): heterojunction technology with silicon-based materials. The Electrochemical Society, 1985, 85: 337

[4] Nathan A, Manku T. Electron drift mobility model for devices based on unstrained and coherently strained $Si_{1-x}Ge_x$ grown on 〈001〉 silicon substrate. IEEE Trans Electron Devices, 1992, 39: 2082

[5] Garchery L, Sagnes I, Warren P, et al. Electron mobility enhancement in a strained Si channel. J Cryst Growth, 1995, 157: 367

[6] Roldan J B, Gamiz F, Cartujo-Cassinello P, et al. Strained-Si on $Si_{1-x}Ge_x$ MOSFET mobility model. IEEE Trans Electron Devices, 2003, 50: 1408

[7] Dhar S, Kosina H, Palankovski V, et al. Electron mobility model for strained-Si devices. IEEE Trans Electron Devices, 2005, 52: 527

[8] Dhar S, Ungersböck E, Kosina H, et al. Electron mobility model for 〈110〉 stressed silicon including strain-dependent mass. IEEE Trans Nanotechnol, 2007, 6: 97

[9] Uchida K, Krishnamohan T, Saraswat K C, et al. Physical mechanisms of electron mobility enhancement in uniaxial stressed MOSFETs and impact of uniaxial stress engineering in ballistic regime. International Electron Devices Meeting, 2005: 129

[10] Chan V, Rim K, Ieong M, et al. Strain for CMOS performance improvement. IEEE Custom Integrated Circuits Conference, 2005: 662

[11] Inc Synopsys SenTaurus Device Version X-2005.10. SenTaurus_manual, 2005: 240

[12] Vandamme E P, Vandamme L K J. Critical discussion on unified $1/f$ noise models for MOSFETs. IEEE Trans Electron Devices, 2000, 47: 2146

[13] Van Langevelde R, Klaassen F M. Effect of gate-field dependent mobility degradation on distortion analysis in MOSFET's. IEEE Trans Electron Devices, 1997, 44: 2044

[14] Ungersbock E, Dhar S, Karlowatz G. Physical modeling of electron mobility enhancement for arbitrarily strained silicon. J Comput Electron, 2007, 6: 55

[15] Mizuno T, Sugiyama N, Tezuka T, et al. High-performance strained-SOI CMOS devices using thin film SiGe-on-insulator technology. IEEE Trans Electron Devices, 2003, 50: 988

[16] Hoyt J L, Nayfeh H M, Eguchi S, et al. Strained silicon MOSFET technology. International Electron Devices Meeting, 2002: 23

[17] Rim K, Chu J, Chen H, et al. Characteristics and device design of sub-100nm strained Si n- and pMOSFETs. IEEE Symposium on VLSI Circuits, Digest of Technical Papers, 2002: 98

[18] Uchida K, Zednik R, Lu C H, et al. Experimental study of biaxial and uniaxial strain effects on carrier mobility in bulk and ultra-thin-body SOI MOSFETs. International Electron Devices Meeting, 2004: 229

[19] Takagi S, Toriumi A, Iwase M, et al. On the universality of inversion layer mobility in Si MOSFET's: Part I - effects of substrate impurity concentration. IEEE Trans Electron Devices, 1994, 41: 2357

应变硅电子迁移率解析模型*

李小健† 谭耀华 田立林

(清华大学微电子学研究所 清华信息科学与技术国家实验室, 北京 100084)

摘要: 提出了一个应变硅沟道电子迁移率解析模型.模型以应变张量为对象研究应变硅沟道电子迁移率,因此与工艺相独立;适用于施加双轴应力及〈100〉/〈110〉方向单轴应力,沟道方向为〈100〉/〈110〉的器件;易于嵌入常用仿真工具中.

关键词: 应变硅; 电子迁移率; 解析模型; n 型场效应管; 单轴应力/应变

PACC: 7220F; 7340Q **EEACC:** 2530F; 2560B

中图分类号: TN301.1 **文献标识码:** A **文章编号:** 0253-4177(2008)05-0863-06

* 国家重点基础研究发展规划资助项目(批准号:2006CB302705)

† 通信作者. Email: lixj03@mails.tsinghua.edu.cn

2007-11-26 收到,2008-01-09 定稿